

Excitation and breakdown of Ar at very high ratios of electric field to gas density

A. V. Phelps* and B. M. Jelenković†

*Joint Institute for Laboratory Astrophysics, University of Colorado
and National Bureau of Standards, Boulder, Colorado 80309*

(Received 11 April 1988)

Spatial distributions of 811-nm emission from the $2p_9$ and $2p_7$ (Paschen notation) levels of Ar have been measured for electrical discharges in Ar at very high ratios of electric field to gas density (E/n) and low nd , where d is the electrode separation. Normalization of the lowest- E/n data to published electron excitation coefficients yields absolute excitation coefficients for $270 < E/n < 43\,000$ Td ($1 \text{ Td} = 10^{-21} \text{ V m}^2$) and for $6.4 \times 10^{19} < nd < 3.5 \times 10^{21} \text{ m}^{-2}$. Direct and cascade excitation of 811-nm emission by electrons calculated using a "single-beam" nonequilibrium electron model is an order of magnitude too small to account for the observed emission at the higher E/n . A model which includes Ar excitation and ionization by Ar^+ and by fast Ar (10–200 eV) is developed to explain the observations. The fast atoms are produced by charge-transfer collisions of Ar^+ with Ar. The estimated excitation by ions is negligible and has the wrong spatial dependence. Using the very limited published cross-section data for 811-nm excitation by fast Ar, the model yields spatial dependencies of emission which agree with experiment, but which are too small by factors ranging from 2.5 at 43 kTd to 10 at 6.3 kTd. This variation in the 811-nm emission with E/n is used to obtain energy-dependent excitation cross sections for fast atoms. The good fit of theory to the experimental spatial dependence near the cathode at the higher E/n shows the importance of ionization of Ar by fast Ar atoms. Excitation by backscattered secondary electrons is an important source of 811-nm emission near the anode. Electrical-breakdown and discharge-maintenance voltages from various experiments, including ours, are compared with the predictions of the model. These analyses show that ionization by ions and fast atoms dominates that by electrons from $E/n > 15$ kTd. The estimated ionization by electrons backscattered from the anode provides sufficient feedback to explain much of the electrical-breakdown data and our discharge-maintenance data. Other breakdown data require either a large yield of ionization by backscattered electrons or a very large ion-induced electron yield at the cathode.

I. INTRODUCTION

This research is an extension to Ar of our previously reported measurements and analyses^{1,2} of the radiation emitted by low current discharges in N_2 at very high ratios of electric field to gas density (E/n) and low gas densities. The previous papers on N_2 will be referred to as I and II, respectively. The principal reasons for selecting Ar were that models³ of positive-ion and fast-neutral-atom behavior are much simpler for Ar than for N_2 and D_2 , and that the relatively large atomic mass lowers the ion velocities and simplifies measurements⁴ of the time-dependent emission. We will show that by constructing a reasonably complete model of Ar^+ -ion and fast-Ar-atom motion, including excitation by the fast Ar atoms, we can obtain good fits to the spatial dependence of emission and to electrical-breakdown voltage data at the higher E/n .

Analyses of electron- and ion-collision processes occurring during electrical breakdown in Ar at very high E/n and low gas densities have been made by Pace and Parker and Bhasavanich and Parker.⁵ These authors used Monte Carlo techniques to simulate the production of ionization by electrons and ions and by electrons reflected from the anode. They consider the contribution of fast neutral atoms to the production of secondary electrons at the cathode, but do not include the ionization of Ar by

fast neutral atoms. Their calculations of electron multiplication at their lower E/n have been compared with our simplified electron model in II.

Models and measurements of ion motion in the cathode fall of discharges in the rare gases^{6–12} are also relevant to the present work. Davies and Vanderslice⁶ measured the ion energy distributions, while Armour *et al.*⁸ extended the measurements to the neutral-atom energy distributions. A number of authors^{6–10} have calculated these distributions. The importance of a proper accounting for the fast neutral atoms has been emphasized by several authors,^{7–9} primarily because they are sources of secondary electrons and of sputtering of the cathode. Particularly useful in our analyses has been the theory of Lawler¹⁰ for ion motion in a spatially uniform electric field. It is important to note the good agreement between theory and experiment in the early results of Davis and Vanderslice,⁶ but the very large discrepancy between these theories and the recent experimental results¹³ obtained by Mase *et al.* and by Ong and Hogan. We have used the theoretical results.

The nonequilibrium behavior of electrons in the cathode fall of Ar discharges has received some attention.¹¹ In addition, experiment and theory¹² have shown that nonequilibrium effects are responsible for oscillatory structure after the electrons leave the cathode, but before

they reach equilibrium.

Because of the extensive discussion in paper I of the experimental apparatus and techniques and in paper II of the electron models used in the present work, we will give only brief summaries of these topics in Secs. II and III A. In Secs. III B and III C we summarize available cross-section data and develop a model for the ion and fast-atom motion and for the resultant production of excited atoms and ionization. The electron and ion-atom models of 811-nm excitation will be compared with experiment in Sec. IV. In Sec. V we compare the predictions of various models of ionization with the measured breakdown and discharge-maintenance voltages.

II. EXPERIMENT AND RESULTS

The experimental apparatus and techniques were discussed in detail in I and will only be summarized here. The discharge was operated between parallel-plane electrodes, which in these experiments were sintered graphite and separated by 38.6 mm. The electrodes were 80 mm in diameter and were surrounded by a close-fitting quartz tube to prevent long-path breakdown. The discharges were operated at currents of $3 \mu\text{A}$ ($2.5 \times 10^{-5} \text{ A/m}^2$) or less so as to prevent space-charge distortion of the spatially uniform electric field and to eliminate nonlinear effects such as gas heating and collisions among excited and/or charged species. The discharge operating voltage was essentially independent of current for current densities of less than 10^{-4} A/m^2 , so that the discharges could be completely characterized by the values of operating voltage versus nd shown by the points in Fig. 1. The argon was stated by the manufacturer to be 99.999% pure, so that for our experiments the principal contamination was from the rate of rise of the system background pressure of 10^{-2} Pa/min . This means that for an hour-long run and for a quenching-rate coefficient for impurities of $10^{-15} \text{ m}^3/\text{s}$, less than 5% of excitation of importance to

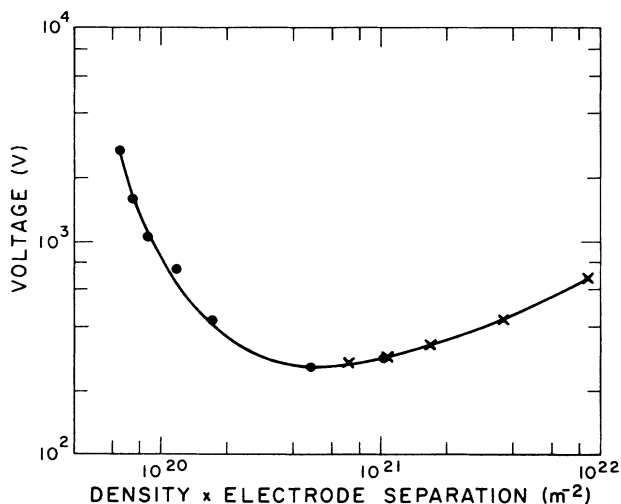


FIG. 1. Discharge-maintenance voltages vs production of gas density and electrode separation for Ar. The \bullet points show our experimental results. The \times points show the results of Penning and Addink (Ref. 17).

the models of Secs. III and IV is lost to quenching by impurities.

Spectral scans from the cathode region of the discharge for $E/n > 5 \text{ kTd}$, obtained using the monochromator arrangement of I, showed that the strongest feature for wavelengths between 250 and 870 nm was unresolved 811.5- and 810.4-nm emission from transitions between the $2p_9$ level (Paschen notation¹⁴) to the $1s_5$ level and from the $2p_7$ level to the $1s_4$ level, respectively. Only Ar lines were observed and at these high E/n the relative spectral intensities from 720 to 820 nm were very close to those shown by Kempter *et al.*¹⁵ in their Fig. 2(g) for collisions of 900-eV Ar with Ar. The lines from Ar^+ between 440 and 490 nm were about an order of magnitude weaker with no correction for the wavelength-dependent sensitivity of the GaAs(Cs) photomultiplier and the monochromator. In this paper we present data only for the unresolved pair of lines at $811 \pm 1 \text{ nm}$. Using the electron-excitation coefficients given by Tachibana¹⁶ for $E/n = 10 \text{ Td}$, one would expect the intensity of the 810.4-nm line to be about 20% of that of the 811.5-nm line. In the case of excitation by fast Ar, the relative level excitation cross-section data of Kempter *et al.*¹⁵ and tabulated transition probabilities¹⁴ lead to approximately equal contributions for the 810.4- and 811.5-nm lines.

The spatial scans were made using an interference filter centered at 808 nm with a bandpass of 10-nm full width at half maximum (FWHM), so that the 811.5- and 810.4-nm lines were detected with very nearly equal sensitivity. The "high-spatial-resolution" slits described in I were used. Data were obtained at the nd values and voltages V_d shown by the points in Fig. 1. Our operating voltages

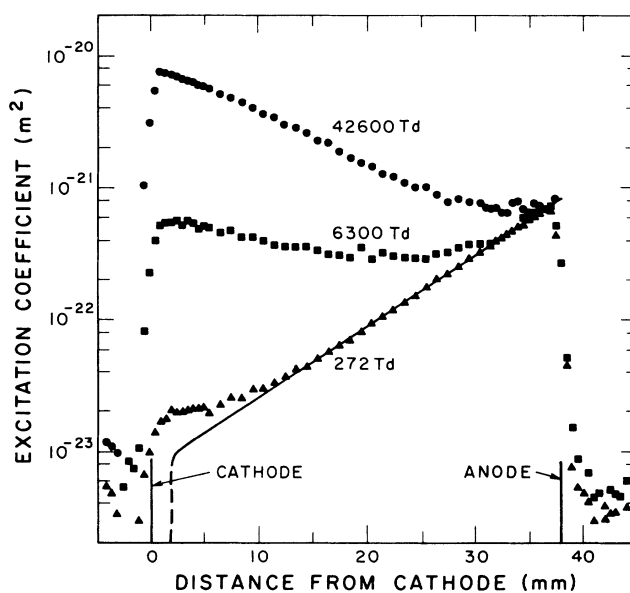


FIG. 2. Apparent excitation coefficient for 811-nm emission vs distance from the cathode. The symbols, E/n in Td, and gas densities in m^{-3} are Δ , 272, 2.7×10^{22} ; \blacksquare , 6300, 3.06×10^{21} ; \bullet , 42600, 1.64×10^{21} . The straight line through the 272-Td data shows the exponential growth of emission with distance. The dashed curve shows the expected nonequilibrium behavior for the 272-Td case.

are in good agreement with previous electrical-breakdown data at the lower E/n using a variety of electrode materials.¹⁷ This agreement is expected since the operating voltage is independent of current. Detailed comparisons at all E/n will be made in Sec. V.

The observed intensities normalized to the gas density versus position are shown in Fig. 2 for three E/n values. As found by several authors¹⁸ for Ne, Kr, and Xe and by us in I for N_2 , the visible emission at $E/n < 1000$ Td increases exponentially with distance from the cathode for most of the electrode gap, e.g., the straight-line fit to the 272-Td data of Fig. 2. The spatial ionization coefficients derived from the exponential growth of emission are shown by the closed circles in Fig. 3. Spatial ionization coefficients determined from current-growth versus electrode-separation experiments¹⁹ are also shown in Fig. 3 by the crosses. As observed in I for N_2 , our ionization coefficients at $E/n > 1$ kTd are significantly lower than the values obtained from current-growth data. We have no explanation for the discrepancy.

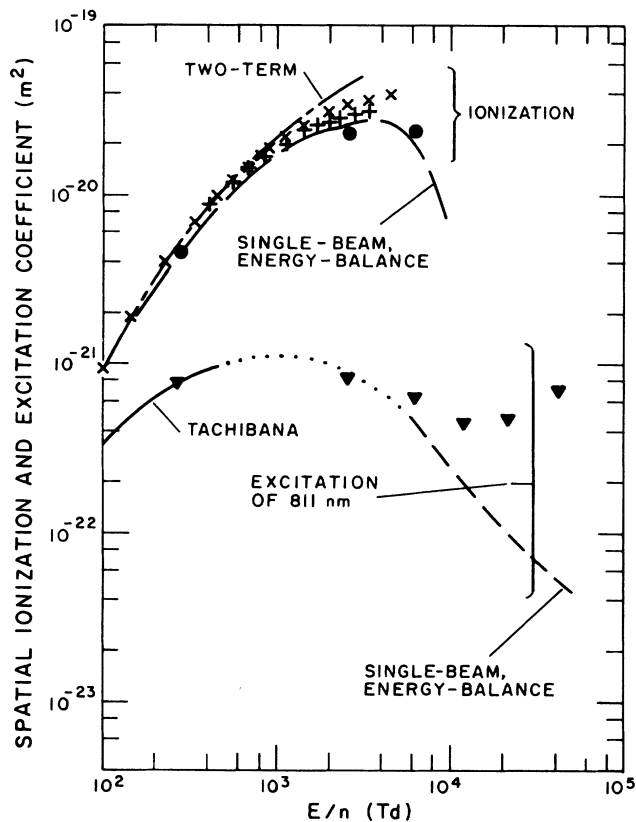


FIG. 3. Spatial ionization and excitation coefficients vs E/n . Spatial ionization coefficient symbols and sources are ●, calculated from the slopes of straight lines through emission data; — — —, calculated using the two-term spherical harmonic expansion (Ref. 16); — — —, calculated using the single-beam, energy-balance model; × and +, coefficients from current growth (Ref. 19). Spatial excitation coefficient symbols and sources are ▼, normalized emission at anode; — — —, measurements by Tachibana (Ref. 16); — — —, calculated using the single-beam, energy-balance model; · · · ·, approximation connecting excitation coefficient curves.

The relative 811-nm emission signals shown in Fig. 2 for 272 Td were extrapolated to the anode, where the total current is assumed equal to the electron current, i.e., we assume that at the anode there is negligible electron-induced emission of ions¹ and negligible ion production by backscattered electrons at this low E/n . After a small (5%) correction for the quenching of excited Ar by Ar, this signal was normalized to the experimental excitation-coefficient data of Tachibana¹⁶ shown by the solid curve in Fig. 3. Equation (7) of I was then used to normalize the remainder of the relative emission signals so as to obtain absolute “apparent” excitation coefficients β^k/n as a function of E/n and nz , where z is the distance from the cathode. Thus

$$\frac{\beta^k}{n}(E/n, nz) = \frac{S_k(E/n, nz)[1/n + 1/n_0]\langle f_i \rangle}{S_k[(E/n)_r, nd][1/n_r + 1/n_0]\langle f_i \rangle_r} \times \left[\frac{\alpha_T^k(E/n)_r}{n} \right] \frac{n_r}{n}, \quad (1)$$

where $S_k(E/n, nz)$ is the measured relative count rate, n is the gas density, n_0 is the density of Ar at which the signal is reduced by 0.5 due to collisional quenching,¹ $\langle f_i \rangle$ is the measured filter transmission, and $\alpha_T^k(E/n)_r$ is Tachibana’s spatially independent excitation coefficient. In Eq. (1) the subscript r is used to designate “reference” values appropriate to the signal at the anode for 272 Td. A quenching density n_0 of $5.6 \times 10^{23} \text{ m}^{-3}$ is calculated from A/k_q , where the quenching-rate coefficient k_q of $6 \times 10^{-17} \text{ m}^3/\text{s}$ is from Chang and Setser²⁰ and the radiative transition probability A is $3.7 \times 10^8 \text{ s}^{-1}$. The resultant quenching corrections are 5% or less for our experiments. In Eq. (1) the ratio of filter-transmission factors was assumed equal to 1, i.e., the effects of changes in the relative intensities of the 811.5- and 810.4-nm lines will be considered elsewhere in our analysis. The effective calibration procedure for the detection system represented by Eq. (1) yields the points of Fig. 2 and the inverted triangles in Fig. 3 for E/n from 2.6 to 42.6 kTd. The “apparent excitation coefficients” shown in Figs. 2 and 3 are the number of excitation events per unit time and per gas atom normalized to the *total-charged-particle* flux density.¹ Alternatively, these coefficients can be regarded as the number of excitation events per unit distance in the field direction per charged particle of either sign passing the observation point and normalized to the gas density. Because of changes in the velocity distribution of the electrons and in the experimentally unknown production of electrons by ionization, it is not possible to express the experimental results in terms of a spatially independent excitation coefficient per unit *electron* flux as is conventionally done^{1,12,16,19} at the lower E/n . The various curves in Fig. 3 will be discussed in Sec. III A.

III. THEORY OF EXPERIMENT

In this section we review briefly the predictions of models of the electron motion and resultant excitation of 811-nm emission. We then develop a model for the Ar^+ produced by ionization and for fast Ar atoms produced in

charge-transfer collisions. We will apply this model in Sec. IV.

A. Ionization and excitation by electrons

We make use of the "single-beam" or monoenergetic-electron-beam model of electron motion based on the energy balance, which we developed in Sec. II A of II. In this model the zeroth and second velocity-moment equations of the electron Boltzmann equation, i.e., the conservation of particles and energy, are solved for the velocity, energy, and collision coefficients of the beam electrons as a function of position. The usefulness of this model has been demonstrated in I and II. Further evidence of its utility is found in the agreement between measured ionization coefficients and the calculated values shown by the long-dashed curve in the upper part of Fig. 3 for $E/n < 8$ kTd. At $1 < E/n < 70$ kTd the single-beam predictions agree with our experiment better than do the results of current-growth experiments¹⁹ shown by the crosses or of two-term spherical harmonic solutions of the Boltzmann equation¹⁶ shown by the single-link chain curve.

Predictions of excitation coefficients using the single-beam, energy-balance model for electrons in Ar are shown by the short dashed curve of Fig. 3 and by the various dashed curves in the lower part of Fig. 4. In

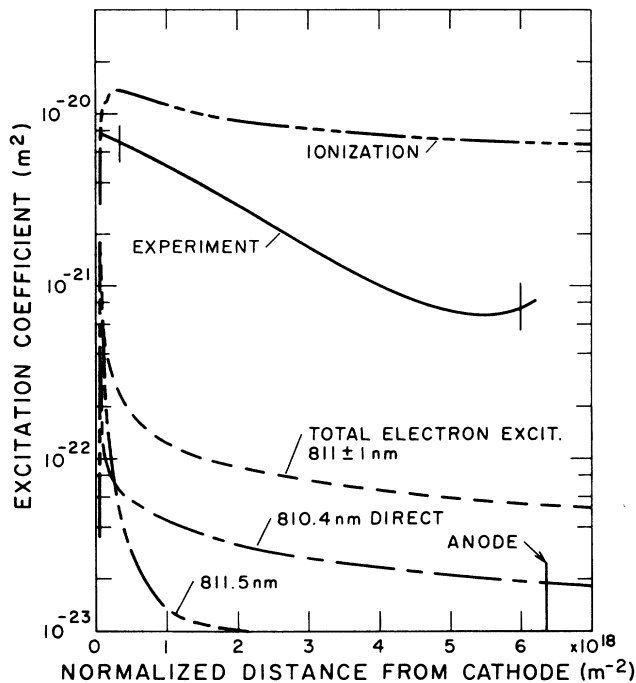


FIG. 4. Apparent excitation and ionization coefficients for 811-nm emission vs normalized distance from the cathode at 42.6 kTd. The symbols and collision process are ———, experiment; ———, calculated ionization by electrons; - - - - -, calculated direct 811.5-nm excitation by electrons; - · - · - ·, calculated 810.4-nm excitation by electrons; · · · · ·, estimated total electron excitation of 811 nm including cascading from 5s and 3d configurations. The vertical bars indicate positions between which we expect distortion of the emission coefficient due to electrodes to be less than 10%.

these calculations we used the electron-Ar momentum-transfer cross section from Hayashi,²¹ an ionization cross section based on Rapp and Englander-Golden and of Schramm *et al.*,²² excitation cross sections for 811.5- and 810.4-nm radiation from Ballou, Lin, and Fajen,²³ and the energy-loss function² from Peterson and Allen.²⁴ We expect the excitation coefficients calculated using the cross sections of Ballou *et al.* to be an upper limit to experiment, since the use of these cross sections in the equilibrium Boltzmann equation at $E/n < 500$ Td gives excitation coefficients significantly larger than those found by Tachibana.¹⁶ The lower dashed curve in Fig. 3 shows that the predictions of the single-beam, energy-balance model for the excitation coefficient at the anode are well below experiment at the higher E/n . Details of the calculation are discussed in connection with Fig. 4.

The triple-link chain curve in Fig. 4 shows the calculated "apparent" ionization coefficient for electrons as a function of normalized distance from the cathode nz . Here, as for excitation, "apparent" is used to indicate that the ionization coefficient varies with position and is normalized to the total current density rather than to the local electron current density. As found in I for N_2 , the ionization coefficient for electrons in Ar is nearly independent of position because of the rough balance between weak electron avalanching and a decreasing ionization cross section with increasing nz .

The solid curve of Fig. 4 shows the measured apparent excitation coefficient for 811-nm emission, while the lower three broken curves show calculated apparent excitation coefficients for the 811-nm lines. The two chain curves show the contributions of "direct" electron excitation, while the short-dashed curve shows the sum of the direct and cascade contributions for the sum of the unresolved lines. The general shapes of the calculated apparent direct-excitation coefficient curves follow from the fact that for the single-beam model,² the excitation coefficient is proportional to the product of the excitation cross section at the electron energy at z and the relative electron current. The narrow maximum in the excitation coefficient curves near $nz = 5 \times 10^{17} \text{ m}^{-2}$ results primarily from the narrow peaks in the 811.5- and 810.4-nm excitation cross sections near 22 eV. These are to be compared to the broad peak in the ionization curve at $nz = 3 \times 10^{18} \text{ m}^{-2}$, which results from the broad peak in the ionization cross section at electron energies near 90 eV.

The lowest curve of Fig. 4 shows the predicted apparent excitation coefficient for the 811.5-nm line by direct electron excitation. In the region near the cathode, the peak in the coefficient is the result of excitation collisions by electrons produced at the cathode, whereas the excitation at nz values greater than about 10^{18} m^{-2} is the result of secondary electrons produced by electron-impact ionization. These secondary electrons are subsequently accelerated rapidly through the region of peak excitation cross section. The latter was calculated using Eq. (18) of II. The single-link chain curve of Fig. 4 shows the calculated apparent excitation coefficient for the 810.4-nm line and includes direct excitation by electrons from both sources. The larger apparent excitation coefficient for the 810.4-nm line at large nz reflects the

fact that the measured cross section²³ for the 810.4-nm line becomes larger than that for excitation of the 811.5-nm line at high electron energies.

Finally, we need to estimate the contribution of cascading to the $2p_7$ and $2p_9$ levels from the $2s_n$ and $3d_n$ resonance levels. The $2s_4$ and $2s_2$ levels of the $3p^5 4s$ configuration and the $3d_2$ and $3s'_1$ levels of the $3p^5 3d$ configuration have large excitation cross sections at high energies²³ because of their large electric dipole transition moments with the ground state. Also, at the gas densities of all of our experiments the Ar is optically thick to the resonance radiation so that these levels decay primarily to the $2p_n$ levels. Examination of the radiative transition probabilities¹⁴ shows that in the absence of collisional mixing, the $2p_7$ level which emits the 810.4-nm line is subject to cascade excitation from the $2s_4$ and $3d_2$ resonance levels, while the 811.5-nm line ($2p_9$ level) is not subject to cascade excitation. Collisional mixing²⁰ is expected to be small at the Ar density of Fig. 4. We use the excitation cross sections from Chutjian and Cartwright²⁵ for energies up to 100 eV and an energy dependence at higher energies based on Peterson and Allen.²⁴ Using radiative transition probabilities¹⁴ to calculate branching ratios and relative excitation cross sections at high energies, we estimate that 30% of the total $2s_n$ and $3d_n$ excitation appears as 810.4-nm emission. When this estimate of the cascade contribution is added to the calculated direct excitation, we obtain the total calculated excitation coefficients shown by the short-dashed curve of Fig. 4. A comparison of this curve with the experimental curve shows that the calculated electron excitation is less than 10% of the experimentally observed values. Also note that the spatial dependence of the calculated total electron excitation shown in Fig. 4 is quite different than that of the observed excitation. When similar estimates are made for other E/n and are extrapolated to the anode, we obtain the short-dashed curve of Fig. 3.

In spite of the approximations of our electron model and gaps in the cross-section data, the calculations presented in this section would seem to rule out excitation by electrons originating at the cathode or by gas ionization as a significant mechanism for production of the 811-nm emission at $E/n > 10$ kTd. The contribution of excitation by backscattered electrons will be discussed in Secs. IV and V.

B. Ion and fast-atom cross sections

The cross section sets which we have assembled from the literature for Ar^+ and Ar collisions with Ar are shown in Figs. 5 and 6. In Fig. 5 the charge-transfer cross section for Ar^+ with Ar at low energies is from Hegerberg *et al.*,²⁶ where agreement with transport data is more important to us than is agreement with beam data.²⁶ At higher energies we have used an average of the somewhat scattered experimental and theoretical results as given by McDaniel.²⁶ The ionization cross section for Ar^+ on Ar is from Sluyters *et al.*²⁷ We find no references to 811-nm or other $2p_n$ -level emission as the result of Ar^+ -Ar collisions.²⁸⁻³¹ We will assume that the 811-nm excitation cross section for Ar^+ on Ar is equal to the

cross section for excitation of the corresponding Ne line, i.e., the 640.2-nm line, by Ne^+ . At 2.5 keV this cross section²⁸ is 1.1 times the cross section for excitation of the 614.3-nm-line level of Ne by Ne^+ . Because of the lack of other information, we will assume the energy dependencies of these two Ne cross sections to be the same. Because of the possible role of resonance and metastable atoms in producing the observed 811-nm excitation, Fig. 5 also shows cross sections for excitation of the uv radiation emitted by resonance states. The sum of the cross sections shown for excitation of the resonance lines of Ar by Ar^+ are from the unpublished results of Iser and Murray.²⁸ Excitation of metastable Ar in Ar^+ -Ar collisions has been observed³² only at energies below 50 eV. We will assume that the curve-crossing model³² used to describe resonance state excitation by Ar^+ also applies to the metastable states, so that the total cross sections for excitation of the metastable and resonance states of the Ar $1s_n$ configuration are approximately equal.

The cross-section set used in our model for fast-Ar collisions with Ar is shown in Fig. 6. The ionization cross

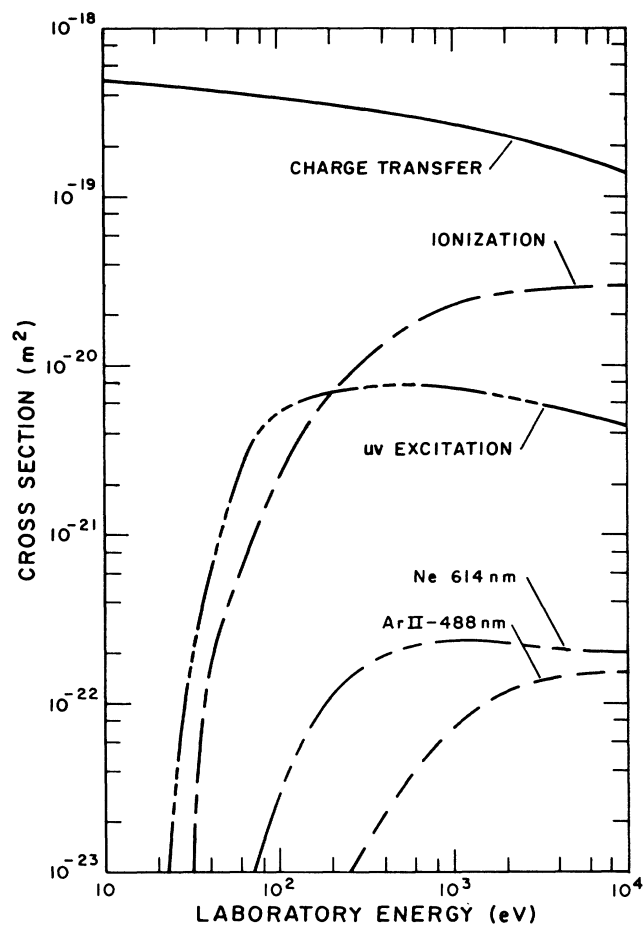


FIG. 5. Cross sections for Ar^+ -Ar collisions vs laboratory energy. The symbols and collision process are —, charge transfer (Ref. 26); ---, ionization (Ref. 27); - - -, Ar II 488-nm excitation (Ref. 28); - · - · -, uv resonance line excitation (Ref. 28); - - - - -, Ne 614.3-nm excitation in Ne^+ -Ne collisions (Ref. 32).

section^{27,33,34} is very close to that for ionization by fast Ar^+ . The momentum-transfer cross section was calculated by Robinson from differential-scattering data.³⁵ The excitation of the $2p_n$ and $3p_n$ levels with emission to the $1s_n$ levels has been reported by Kempter *et al.*¹⁵ and Neuman,³⁶ respectively. The only energy-dependent cross section given¹⁵ for the Ar $2p_n$ lines is that shown in Fig. 6 for the 795-nm line. The curve for the combined 811.5- and 810.4-nm lines shown by the triple-link chain curve in Fig. 6 is obtained by multiplying the 795-nm cross sections by the ratio of the 811-nm to 795-nm intensities shown for 900-eV laboratory energy in Fig. 2(g) of Ref. 15. The sum of the cross sections for excitation of the 104.8- and 106.7-nm resonance lines³⁷ is approximately equal to the ionization cross section. A significant fraction of the resonance line production is attributed¹⁵ to cascading from higher levels.

Cross sections for near-threshold excitation of metastable Ar in Ar-Ar collisions has been measured by beam

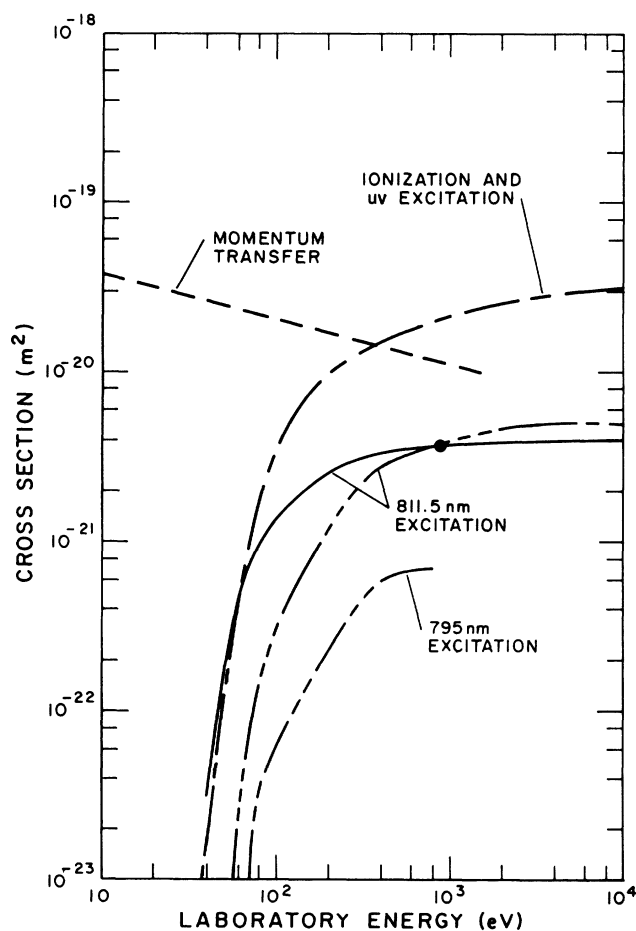


FIG. 6. Cross sections for Ar-Ar collisions vs laboratory energy. The symbols and collision process are — — —, momentum transfer (Ref. 35); — · — · —, ionization and uv excitation; — — — —, 811-nm excitation scaled from 795-nm data (Ref. 15); — — — —, 811-nm excited adjusted to fit our experiment and the point (●) at 900 eV (Ref. 15); · · · · ·, 795-nm excitation (Ref. 15).

techniques³⁴ and inferred from the growth of ionization in shock tubes,³⁸ but are not available at the higher energies of interest to us. Low-angle, high-energy resolution measurements³⁹ of the scattering of Ar by Ar demonstrate the dominance of excitation to the $1s$ and $2p$ configurations of Ar at high energies, but neither experiments nor theory^{39,40} give information as to the ratio of cross sections for metastable and resonance-line excitation. As for Ar^+ , we estimate the cross sections for excitation of Ar to the metastable states by fast Ar to be equal to those for resonance-line excitation in Ar-Ar collisions.

C. Ion and fast-atom model

This section contains a simple model of the motion and reactions of the Ar^+ and fast-Ar atoms in the presence of the spatially uniform electric field. We take advantage of the short mean free paths of the Ar^+ in Ar and assume that the ions are in equilibrium¹⁰ with the gas at the applied E/n . Charge-exchange collisions produce fast-Ar atoms which are assumed to have the same energy distribution as the equilibrium Ar^+ energy distribution. Rather than solve the spatial and energy-dependent Boltzmann equation for the fast atoms, we will model the behavior of only the fast Ar which have not had a collision. Each collision of a fast-Ar atoms with Ar is assumed to result in loss of the fast atom and the production of a slow atom which is subsequently ignored. This approximation is believed to be satisfactory for the modeling of our excitation experiments, because most of the fast atoms are produced with energies below 200 eV and because the excitation and ionization cross sections shown in Fig. 6 decrease rapidly with energy below 200 eV.

The electron motion will be calculated using the single-beam, energy-balance model derived and discussed in Sec. II A of II and used in Sec. III A of this paper. According to this model the spatial growth of the steady-state electron flux density Γ_e is determined by the sum of the contributions of ionization collisions of electrons, Ar^+ , and fast Ar with Ar. Thus

$$\frac{d\Gamma_e}{d\xi} = Q_e^i(\varepsilon)\Gamma_e(\xi) + \frac{\alpha_p^i}{n}(E/n)\Gamma_p(\xi) + \frac{\alpha_f^i}{n}(E/n)\Gamma_f(\xi). \quad (2)$$

Here $\xi = nz$ is the normalized distance or column density measured from the cathode, $Q_e^i(\varepsilon)$ is the cross section for ionization by electrons, $\alpha_p^i(E/n)/n$ is the spatial ionization coefficient for the Ar^+ , $\alpha_f^i(E/n)/n$ is the spatial ionization coefficient for fast neutral atoms, and $\Gamma_p(\xi)$ and $\Gamma_f(\xi)$ are the particle flux densities for the Ar^+ and for the fast neutral atoms. The equation for the spatial growth of the energy ε of the electron beam includes the energy gain from the field and the energy lost in inelastic collisions. Since the model assumes a single energy for all electrons, this equation also includes the energy required to raise the energy of new electrons produced by ionization from essentially zero to the beam energy, i.e.,

$$\frac{d\varepsilon}{d\xi} = \frac{eE}{n} - \sum_{k,i} \varepsilon_m Q_e^m(\varepsilon) - \varepsilon \left[Q_e^i(\varepsilon) + \frac{\alpha_p^i}{n} \frac{\Gamma_p(\xi)}{\Gamma_e(\xi)} + \frac{\alpha_f^i}{n} \frac{\Gamma_f(\xi)}{\Gamma_e(\xi)} \right]. \quad (3)$$

Here the products of threshold energy ε_m and cross section Q_e^m are summed over all excited states k and ionization states i . In Eq. (3) we have neglected the loss of energy by electrons in elastic collisions, as is appropriate to the high E/n of interest.² As in I and II, the α/n are described as “spatial” reaction or excitation coefficients and are the number of collision events per unit distance in the direction of ion drift. The word “spatial” also distinguishes these coefficients from “temporal” reaction or rate coefficients. A less descriptive terminology sometimes used is “Townsend-type” coefficient, because of the Townsend ionization coefficient.¹² The calculation of these coefficients will be discussed below.

The steady-state continuity equations for the Ar^+ flux density $\Gamma_p(\xi)$ and the fast-Ar flux density $\Gamma_f(\xi)$ in the present model are

$$-\frac{d\Gamma_p}{d\xi} = +Q_e^i(\xi)\Gamma_e(\xi) + \frac{\alpha_p^i}{n}(E/n)\Gamma_p(\xi) + \frac{\alpha_f^i}{n}(E/n)\Gamma_f(\xi) \quad (4)$$

and

$$-\frac{d\Gamma_f}{d\xi} = +Q_{CT}\Gamma_p(\xi) - \frac{\alpha_f^a}{n}(E/n)\Gamma_f(\xi), \quad (5)$$

where

$$\frac{\alpha_f^a}{n}(E/n) = \frac{\alpha_f^m}{n}(E/n) + \frac{\alpha_f^i}{n}(E/n) + \frac{\alpha_f^k}{n}(E/n). \quad (6)$$

Equation (4) states that the increase in the Ar^+ flux density is due to the production of Ar^+ by ionizing collisions of electrons, ions, and fast atoms with Ar. Equation (5) states that the growth of the fast-atom flux is due to the production of fast atoms by charge-transfer collisions and their loss by any collision process. The negative signs on the left-hand sides of Eqs. (4) and (5) result from the flow of positive ions and, therefore, fast neutrals toward the cathode, i.e., toward smaller ξ . Here Q_{CT} is the charge-transfer cross section for Ar^+ -Ar collisions, α_f^a/n is the average cross section for the attenuation of fast neutrals, α_f^m/n is the average cross section for momentum transfer

in Ar-Ar collisions, and α_f^k/n is the average cross section for excitation of Ar by the fast Ar in process k . Equations (2) and (4) are consistent with $\Gamma_e + \Gamma_p = \Gamma_T$, where Γ_T is the total charged-particle flux and is independent of position.

The spatial ionization and excitation coefficients for Ar^+ are given by

$$\frac{\alpha_p^x}{n}(E/n) = \frac{\int dv v Q_p^x(v) f(v)}{\int dv v_z f(v)} = (kT_+)^{-1} \int_0^\infty d\varepsilon Q_p^x(\varepsilon) \exp\left[-\frac{\varepsilon}{kT_+}\right], \quad (7)$$

where x is either k for excitation or i for ionization and

$$(kT_+)^{-1} \exp(-\varepsilon/kT_+)$$

is the normalized steady-state energy distribution for the Ar^+ as given by several authors.^{6,9,10} The ion “temperature” T_+ is given by $kT_+ = eE/(nQ_{CT})$, and the corresponding drift velocity is

$$W_+ = (2eE/\pi mn Q_{CT})^{1/2},$$

where e is the electron charge and k is Boltzmann’s constant. Note that the theoretical Ar^+ energy distribution¹⁰ is a one-dimensional distribution, i.e., it is a δ function in directions perpendicular to the electric field and a Maxwellian in the direction of the field. The $\alpha_p^{i,k}/n$ are independent of position and are functions of E/n , since kT_+ is a function of E/n . Table I gives values of α_p^i/n used in our model.

The solid and long-dashed curves of Fig. 7 shows the theoretical^{10–16} steady-state ion drift velocity W_+ and kT_+/e as a function of E/n for Ar^+ in Ar as calculated using the charge-transfer cross sections of Fig. 5. At the E/n of interest the thermal motion of the atoms can be neglected. The short-dashed curve shows experimental⁴¹ drift velocities which are in good agreement with calculations. Note that the calculated values of kT_+ are significantly larger than the kT_{eff} calculated from drift velocities.⁴¹

Theory¹⁰ shows that for a spatially uniform production of ionization, the Ar^+ reaches 80% of its equilibrium drift velocity in a distance of $1.5\lambda_p$. The single- and double-link curves of Fig. 7 show the mean free paths for the Ar^+ ($\lambda_p = 1/nQ_{CT}$) and fast Ar ($\lambda_f = 1/\alpha_f^a$) for the gas densities of our experiments. Since Fig. 4 shows that

TABLE I. Excitation and ionization coefficients calculated from published cross sections discussed in detail in Sec. III B. Note that $4.9[-22]$ means 4.9×10^{-22} .

| E/n (kTd) | α_f^k/n (m ²) | α_f^i/n (m ²) | α_p^{uv}/n (m ²) | α_p^i/n (m ²) | α_p^k/n (m ²) | α_f^a/n (m ²) |
|----------------|-------------------------------------|-------------------------------------|--|-------------------------------------|-------------------------------------|-------------------------------------|
| 42.6 | 4.9[-22] ^a | 3.8[-21] | 3.7[-21] | 2.8[-21] | 4.3[-23] ^b | 2.4[-20] |
| 22 | 1.45[-22] ^a | 1.5[-21] | 2.2[-21] | 1.0[-21] | 1.4[-23] ^b | 2.4[-20] |
| 6.3 | 2.5[-24] ^b | 4.0[-24] | 3.0[-22] | 4.9[-23] | 2.7[-25] ^b | 3.0[-20] |

^a α_f^k/n calculated using — — curve of Fig. 6.

^b α_p^k/n calculated using 614.3-nm excitation cross section for Ne^+ on Ne from Ref. 28 and Fig. 5 as discussed in text.

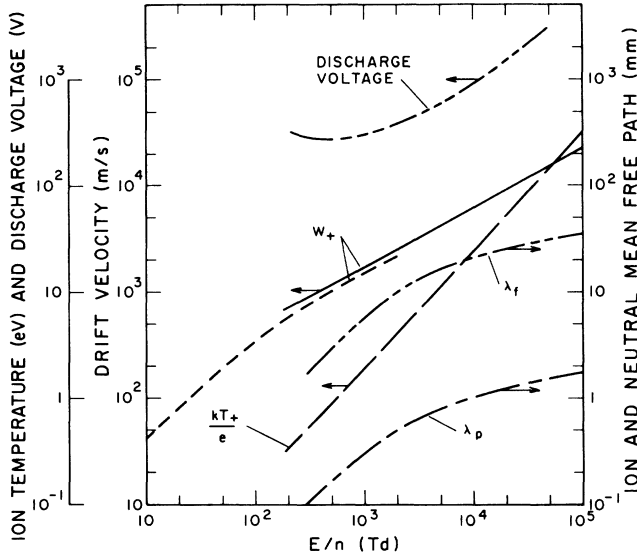


FIG. 7. Transport and discharge parameters for Ar^+ in Ar as a function of E/n . The symbols and parameters are —, calculated ion drift velocity W_+ ; - - -, experimental drift velocity; — · —, energy equivalent temperature kT_+/e ; - - - -, Ar^+ mean free path; - - - -, fast-neutral-atom mean free path; · · · · ·, discharge voltage.

the ionization is nearly uniform in our high- E/n experiments, we conclude that the ions reach equilibrium in 10% or less of the gap.

The spatial reaction coefficients describing ionization, momentum-transfer, and excitation collisions for our model of the fast-atom motion are given by

$$\frac{\alpha_f^x}{n}(E/n) = (kT_+)^{-1} \int_0^\infty d\varepsilon Q_f^x(\varepsilon) \exp\left[-\frac{\varepsilon}{kT_+}\right], \quad (8)$$

where $Q_f^x(\varepsilon)$ is the cross section for the process x . Here x is i for ionization, a for attenuation by any kind of collision, or k for excitation. These α^x/n are independent of position and are functions of E/n through kT_+ . Tables I and II give values of α_f^i/n and α_f^k/n used in our model.

The four boundary conditions appropriate to the four first-order differential equations, Eqs. (2)–(5), describing our experiment are

$$\begin{aligned} \Gamma_e(0) &= \gamma_p \Gamma_p(0) + \gamma_f \Gamma_f(0), \\ \varepsilon(0) &= \varepsilon_0, \end{aligned} \quad (9)$$

TABLE II. Excitation coefficients and flux ratios for model. Note that 6.3[19] means 6.3×10^{19} .

| E/n (kTd) | nd (m^{-2}) | α_f^k/n (m^2) | $\frac{\Gamma_f(0)}{\Gamma_p(0)}$ |
|----------------|-----------------------------|------------------------------------|-----------------------------------|
| 42.6 | 6.3[19] | 1.1[–21] | 6.0 |
| 22 | 7.3[19] | 4.9[–22] | 8.3 |
| 6.3 | 1.23[19] | 2.4[–23] | 15.4 |

and

$$\Gamma_p(d) = \Gamma_f(d) = 0, \quad (10)$$

where γ_p and γ_f are the yields of electrons at the cathode due to the arrival of Ar^+ and fast Ar, respectively, and where ε_0 is some convenient electron energy, e.g., 1 eV. Here we have neglected photon-induced electron emission as too inefficient⁴² to compete with the ion- and fast-atom-induced emission at high E/n . Equation (9) states that enough electrons must be released from the cathode by the arriving ions and fast atoms to maintain the discharge. The yield of electrons per incident Ar atom for energies of about 100 eV is about an order of magnitude lower than for Ar^+ of the same energy.⁴³ We will therefore simplify the analysis by assuming that $\gamma_f = 0$ and regard γ_p as an effective value. This assumption will need to be reexamined as our models improve and secondary emission data for fast-Ar atoms on graphite become available. We assume no electron-induced emission of ions or fast atoms from the anode.¹ We will consider the question of ion production near the anode by backscattered electrons in Secs. IV and V.

The apparent spatial excitation coefficients $\beta^k(\xi)/n$ required for comparison with experiment are obtained by recalling their basic definition as the number of excitation events per unit time and per gas atom normalized to the total charged-particle flux density. For the electron-beam model described by Eqs. (2) and (3), this means

$$\begin{aligned} \beta_e^k(\xi, E/n)/n &= Q_e^k(\xi) \Gamma_e(\xi) / \Gamma_i \\ &= Q_e^k(\xi) \Gamma_e(\xi) / \Gamma_e(nd), \end{aligned} \quad (11)$$

where Γ_i is the steady-state current density per unit charge. For Ar^+ the apparent excitation coefficient is

$$\begin{aligned} \frac{\beta_p^k}{n} \left[\xi, \frac{E}{n} \right] &= \frac{\alpha_p^k}{n}(E/n) \frac{\Gamma_p(\xi)}{\Gamma_i} \\ &= \frac{\alpha_p^k}{n}(E/n) \frac{\Gamma_p(\xi)}{\Gamma_e(nd)}, \end{aligned} \quad (12)$$

where $\alpha_p^k(E/n)/n$ is given by Eq. (7) with $Q_p^k(\varepsilon)$ substituted for $Q_p^i(\varepsilon)$. Similarly, for fast Ar the apparent excitation coefficient is

$$\begin{aligned} \frac{\beta_f^k}{n} \left[\xi, \frac{E}{n} \right] &= \frac{\alpha_f^k}{n}(E/n) \frac{\Gamma_f(\xi)}{\Gamma_i} \\ &= \frac{\alpha_f^k}{n}(E/n) \frac{\Gamma_f(\xi)}{\Gamma_e(nd)}, \end{aligned} \quad (13)$$

where α_f^k/n is calculated using Eq. (8) with $x = k$.

It is of interest to point out that for a given gas and a given set of electrode properties, the scaling parameters for Eqs. (2)–(13) are E/n and nd . When expressed in terms of $V_d = Ed$ and nd , these are the parameters which appear in Paschen's law,¹² which states that at breakdown V_d is a function of nd (see Sec. V). We have used several different approaches in solving Eqs. (2)–(13). We will present the results of the numerical solutions in Secs. IV and V. Some details of the calculation are presented

in the Appendix.

Before making comparisons with experiment, it is instructive to consider analytic solutions appropriate for high E/n and small ionization by the Ar^+ and fast Ar. The spatial dependence of the apparent electron-ionization coefficient at high E/n was found in II and in Fig. 4 to be nearly independent of position and roughly equal to the maximum in the ionization cross section. Ionization by Ar^+ and fast Ar is small for $E/n < 20$ kTd and for small nd . Thus, when $Q_e^i(\epsilon)\Gamma_e(nz) = Q_{\max}^i \Gamma_e(nd)$ and the heavy-particle ionization terms are small in Eq. (4), $\Gamma_p(z)$ is given by

$$\Gamma_p(z) = Q_{\max}^i \Gamma_e(nd) n \times (d - z) \quad (14)$$

and, in the limit of small attenuation of the fast neutrals, Eq. (5) gives

$$\Gamma_f(z) = [Q_{\text{CT}} Q_{\max}^i \Gamma_e(nd) / 2] n^2 (d - z)^2. \quad (15)$$

In this high- E/n and low- nd limit, substitution of Eqs. (14) and (15) into Eqs. (12) and (13) for the 811-nm excitation then gives linear and quadratic variations with distance from the anode of β_p^k/n and β_f^k/n , respectively. This difference in the spatial dependence of 811-nm excitation by Ar^+ collisions versus 811-nm excitation by fast Ar provides one method of distinguishing between these two excitation sources.

IV. COMPARISON OF MODELS WITH EMISSION EXPERIMENT

The results of the numerical solutions of Eqs. (2)–(15) using the coefficients of Tables I and II are compared with the 811-nm emission experiments in Figs. 8–10.

A. 42.6-kTd measurements

1. Excitation by fast atoms and ions

The solid curve of Fig. 8, showing our experimental results, was obtained by drawing a smooth curve through the data of Fig. 2 for $E/n = 42.6$ kTd. The short-dashed curve of Fig. 8 shows the results of a numerical calculation for 42.6 kTd in which the heavy-particle ionization terms α_p^i and α_f^i have been included in Eq. (4), but omitted from Eqs. (2) and (3). As shown in the Appendix, the resultant error in the excitation coefficients is small. This is apparently because electron avalanching is small at high E/n and because of the normalization of the excitation coefficient to the total current. The double-link chain curve shows that the additional effect of omitting the fast-atom ionization terms from Eq. (4) is to produce too slow a variation in the excitation coefficient with position. Although not shown, the effect of omitting ionization by fast ions is small because of the significantly larger number of fast atoms than ions produced by the charge-transfer process and because of the comparable ionization cross sections for Ar^+ and Ar shown in Figs. 5 and 6, respectively. The ratio of the fast-atom flux to the ion flux is shown by the single-link chain curve in Fig. 8. At the high E/n and low nd of Fig. 8, the energy-balance and momentum-balance models of electron motion dis-

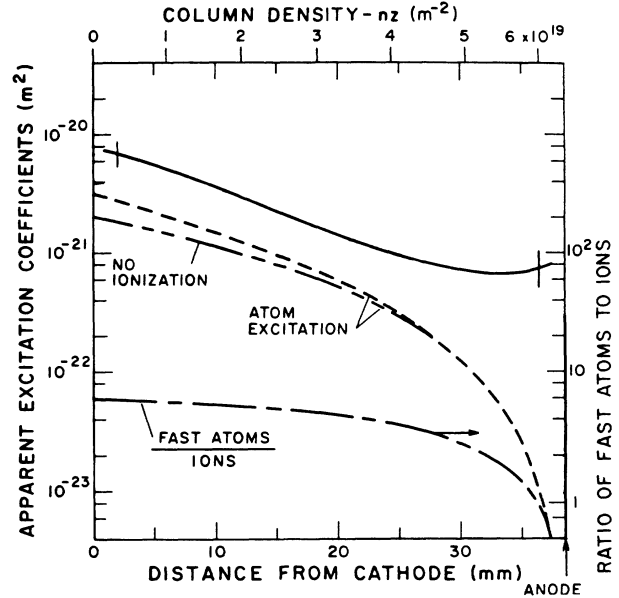


FIG. 8. Comparison of experimental and calculated apparent spatial excitation coefficients for 811-nm emission vs distance from the cathode for $E/n = 42.6$ kTd. The curves and meanings are —, experiment from Fig. 2; - - -, solution of Eqs. (2)–(13) discussed in text; - - - - -, model without ionization by fast atoms; — — —, ratio of fast-atom flux to ion flux. The vertical bars are as in Fig. 4.

cussed in II give essentially the same results because the electrons are very nearly in free-fall motion.

From Fig. 8 we see that when ionization by the fast atoms is included in the model the agreement between the observed and calculated spatial dependence of the 811-nm emission is significantly improved and is good from near the cathode to about 60% of the gap distance. However, the magnitude of the calculated curve is only about 40% of the experimental values. Here we note that the cross section shown by the triple-link chain curve in Fig. 6 and used to calculate the α_f^k/n values in Table I is really based on the single point of Kempter *et al.*¹⁵ at 900 eV for the 811-nm excitation, so that a much larger cross section for 811-nm excitation by fast Ar at energies in the 100 eV region is possible. The solid curve in Fig. 6 shows a cross section which is chosen to give good agreement ($\pm 10\%$) with spatial excitation coefficients derived from our experiments for $E/n \geq 6.3$ kTd and still passes through the data point¹⁵ at 900 eV. Table II lists the 811-nm excitation coefficients α_f^k/n calculated using the cross section shown by the solid curve of Fig. 6. Table II also lists the calculated ratios of fast-atom flux to positive-ion flux at the cathode and the values of nd used in these experiments.

As discussed in Sec. III B the contribution of Ar^+ ions to the production of the 811-nm emission is estimated using the cross section for the 614.3-nm transition in Ne excited by Ne^+ shown in Fig. 5. The resultant 811-nm production by ions is less than 3% of the experimental values.

2. Excess excitation near the anode

There is a large discrepancy between the predictions of the fast atom model of 811-nm excitation presented in Fig. 8 and experiment in the vicinity of the anode. From the difference between the observed values of β^k/n and the calculated sum of β_p^k/n and β_f^k/n after adjustment to fit experiment near the cathode, we find the magnitude and spatial distribution of the required emission coefficient. Although we have not found a satisfactory quantitative agreement between theory and experiment for this emission at $E/n = 42.6$ kTd, it seems worthwhile to go through the estimates.

The only qualitatively satisfactory explanation for the excess 811-nm signal near the anode appears to be excitation by backscattered electrons produced by the high-energy electrons striking the anode. In order to explain the observed excess by this process, we require a spatially integrated production of 811-nm excitation of about 0.008 photons per electron striking the anode and a range of the average electrons in the retarding field of 7.2×10^4 V/m of about 6 mm. This corresponds to an average energy of about 400 eV.

We can rule out a significant contribution of those backscattered electrons with energies below 50 eV, customarily labeled secondary electrons,⁴⁴ since the maximum distance a 50-eV electron can travel against the applied field is only 0.7 mm, and since we see no peak in the emission very close to the anode, such as was found¹ for N_2 . Furthermore, experiments show that only about 10% of the secondaries typically have energies above the excitation potential for 811-nm excitation,⁴⁴ and that the yield of secondary electrons is only 0.25 for our type of graphite.⁴⁵

We now consider the higher-energy group of electrons labeled backscattered electrons.⁴⁴ As outlined in II, calculations of 811-nm excitation by backscattered electrons were made using our single-beam electron model. Cascading was included as discussed in Sec. III A of the present paper. For 42.6 kTd, the calculated photon yield⁴⁶ is 0.01 photon per 400-eV electron leaving the normal to the anode. These relations show that in order to explain the observations we require 0.5 to 1 backscattered electron for each electron reaching the anode. The calculated energy for electrons striking the anode for $E/n = 42$ kTd is 1300 eV, for which experiments⁴⁷ with carbon of unspecified composition give backscattered electron ($\epsilon > 50$ eV) yields of 0.08 to 0.25. Thus our calculation of the emission coefficient caused by backscattered electrons is a factor of 2 to 10 too small to account for the excess 811-nm emission near the anode. It appears to us that the most likely sources of error in this model are the estimates of the cascade contribution to the 811-nm excitation and the yield of backscattered electrons.

We have no other candidate for this excess emission. For example, while the production of additional ionization near the anode discussed in Secs. V B and V C increases the 811-nm signal⁴⁸ generated by fast-atom collisions by about a factor of 2 at 3 mm from the anode, this calculated signal is a factor of 5 below the measured signal and has the wrong dependence on position. Obvi-

ously we need more detailed calculations of the backscattering, including the contribution of repeated backscattering from the anode, the effects of electron emission from the anode at an angle to the normal, and more complete data on backscattered electrons. Measurements of the emission of lines excited only by electrons would be of help in resolving this problem, as was the case in I for the 391.4-nm band of N_2 .

B. 22-kTd measurements

Our second comparison of experiment and models is intended to demonstrate the better agreement with experiment of the quadratic spatial dependence of 811-nm excitation by fast neutral atoms as compared to the linear dependence of excitation by ions. Thus Fig. 9 shows measured and calculated apparent 811-nm excitation coefficients on a linear scale versus distance from the cathode for 22 kTd. The points are the experimental values. The solid curve is that calculated using the adjusted fast-atom cross sections shown by the solid curve of Fig. 6 and the excitation coefficient of Table II, while the long-dashed curve is that calculated assuming only excitation by fast ions and using an α_p^k/n value adjusted to fit experiment at the cathode. We see that, except for points near the anode, the agreement between experiment

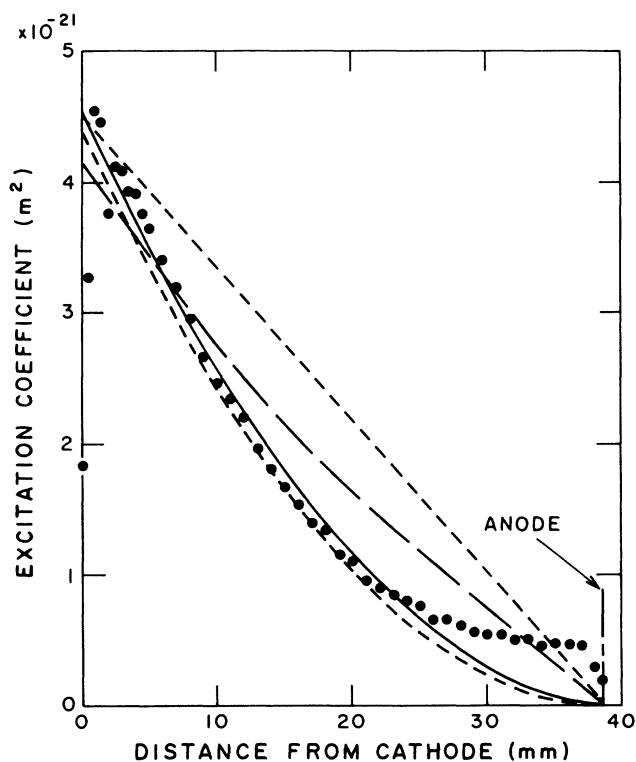


FIG. 9. Comparison of experimental and calculated apparent spatial excitation coefficients for 811-nm emission vs distance from the cathode for $E/n = 22$ kTd. The points \bullet show the experimental results. The curves and meanings are —, solution of Eqs. (2)–(13) discussed in text; — —, model with excitation by fast atoms replaced by excitation by ions and adjusted cross section; - - -, calculations using Eqs. (14) and (15).

and the model is much better for excitation by fast Ar than for excitation by Ar^+ .

The upper and lower short-dashed curves in Fig. 9 are calculated using the approximate models for 811-nm excitation represented by Eq. (14) for ions and Eq. (15) for fast atoms, respectively. The curve for excitation by ions was calculated by increasing the rate coefficient α_p^k/n from Table I by an order of magnitude, while the curve for 811-nm excitation by fast neutral atoms was calculated using the α_f^k/n from Kempter *et al.*¹⁵ listed in Table I. The agreement using Eq. (15) for excitation by fast neutral atoms is better than expected in view of the marginal applicability of the assumptions made in deriving Eqs. (14) and (15). This agreement is, in part, the result of too large an ionization coefficient and too small an excitation coefficient. The upper short-dashed curve shows again that the ion-excitation model represented by Eq. (14) is far less satisfactory than is the fast-atom model.

The yield of 811-nm photons per electron incident on the anode and the electron range required to explain the excess emission near the anode for 22 kTd is very much the same as for 42.6 kTd, i.e., 7.5×10^{-3} photons per electron striking the anode and a backscattered electron mean energy of 320 eV. In this case the calculated yield of 811-nm photons per electron leaving normal to the anode of about 0.02 means that consistency would require 0.2 to 0.4 backscattered electron per incident electron or the equivalent for repeated backscattering. For the calculated incident energy of 560 eV, the measured yields⁴⁷ vary from 0.1 to 0.4. Thus by assuming limiting values one can obtain consistency between experiment and the backscattering model.

C. 6.3-kTd measurements

The final comparison between experiment and the models of the 811-nm emission is made in Fig. 10, where $E/n = 6.3$ kTd. The contribution of electron excitation β_e^k/n , including the 30% cascade contribution, is shown by the dashed curve and is dominant near the anode. Excitation due to backscattered electrons is not expected to be significant since the calculated energy of electrons striking the anode is only 40 eV. The contribution of fast-atom excitation of 811-nm emission calculated using the α_f^k/n excitation coefficient of Table I is shown by the single-link chain curve. In order to fit the observed emission near the cathode one has to increase the 811-nm excitation coefficient by fast Ar by a factor of about 10 at Ar energies corresponding to $kT_+/e = 16$ eV. The resultant cross section is shown by the solid curve of Fig. 6 and yields the α_f^k/n values in Table II. The apparent excitation coefficient β_f^k/n for the fast neutral atoms is shown by double-link chain curve of Fig. 10. The agreement of the sum of these contributions to the apparent excitation coefficient with experiment is very good. In particular, this agreement near the anode confirms our calibration and points to problems with the electron backscattering model at the higher E/n .

Spatial distributions of 811-nm emission were also obtained at 2.6 and 12 kTd, but were not analyzed in detail. Qualitatively, the data for 12 kTd look much like the 22-

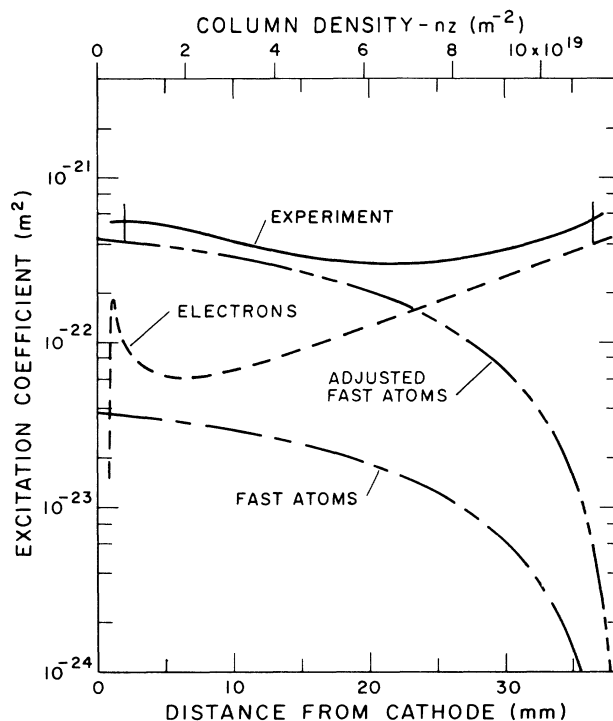


FIG. 10. Comparison of experimental and calculated apparent spatial excitation coefficients for 811-nm emission vs distance from the cathode for $E/n = 6.3$ kTd. The curves and their meanings are —, experiment from Fig. 2; ---, calculated electron excitation; - - -, solution of Eqs. (2)–(13) discussed in text; — · —, solution of Eqs. (2)–(13) text with adjusted cross section for excitation of 811 nm by fast Ar as shown in Fig. 6. The vertical bars are as in Fig. 4.

kTd data, but with a relatively large contribution from electrons near the anode. The 2.6-kTd data resembles the 272-Td data, but with a relatively much larger signal near the cathode. Note that it is possible to fit the emission near the cathode at 2.6 kTd by postulating a peak in the cross section for 811-nm excitation in Ar-Ar collision having an integrated magnitude of roughly 5×10^{-21} $\text{m}^2 \text{eV}$ at 30–50-eV laboratory energy. Such a peak makes no significant contribution to the calculated emission at 272 Td, so that we have no explanation for the excess emission near the cathode at this E/n .

D. Excitation by excited atoms

We will now discuss the possible contribution of fast atoms excited to the 1s metastable and resonance levels of Ar in collisions of Ar^+ or fast Ar with Ar to the production of the observed 811-nm emission at high E/n . Such excited atoms could have significantly larger cross sections for excitation of 811-nm emission than the fast ground-state atoms considered thus far. We do not expect that the fast atoms excited to resonance levels in charge-transfer collisions will cause further excitation because of their short radiative lifetimes and the small probability of reabsorption of their Doppler-shifted emission resulting from the large kinetic energies acquired from short-range excitation collisions.^{39,40} If we assume

from Sec. III B that the cross section for fast metastable production is the same as shown for resonance photons in Fig. 5 and, as an upper limit, assume that each fast metastable produces a 811-nm photon, then the calculated 811-nm emission for 42.6 kTd is about 30% of the experimental value at the cathode shown in Fig. 8. The basic reason for this small signal is that even this very large assumed metastable production cross section is small compared to the charge-transfer cross section shown in Fig. 5. Since the efficiency of 811-nm excitation by fast-Ar metastable atoms is unlikely to be near unity, we expect that the production of 811-nm emission by metastable atoms is considerably less than that observed in our experiments.

V. BREAKDOWN AND DISCHARGE MAINTENANCE

Comparisons of experimental and calculated electrical breakdown and low-current discharge-maintenance data are presented in Fig. 11. The points show experimental results from Fig. 1 and from various authors.^{5,17,49} Here we have plotted the values of nd required for breakdown as a function of the E/n , instead of the usual plot of breakdown voltage versus nd . We will usually refer to the breakdown voltage and to processes occurring at breakdown rather than those of low-current discharge maintenance, since the measured voltages are the same to within a few percent for both phenomena. The discharge currents in our experiments are small enough so that multistep ionization phenomena are not significant (see Sec. II).

A. Ionization by electrons only

Most models for breakdown¹² consider only electron-impact ionization of the gas and the production of second-

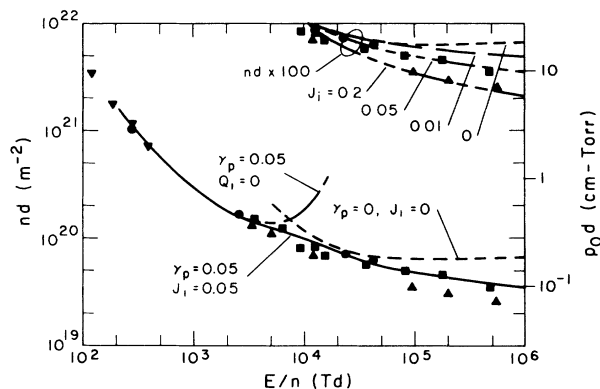


FIG. 11. Experimental and calculated values of the product of gas density n and electrode separation d for breakdown or for low current, steady-state discharges vs E/n in Ar. Note that for the data and curves in the upper right-hand corner the nd values have been multiplied by 100. The symbols, surfaces, and sources are ●, sintered graphite (Fig. 1); ■, steel from Guseva (Ref. 45); ▼, iron from Penning and Addink (Ref. 17); ▲, stainless steel from Bhasavanich and Parker (Ref. 5). The calculated curves and parameters are —, $\gamma_p=0.05$ and $J_i=0.05$; ---, $\gamma_p=0.05$, $J_i=0$, and no ionization by atoms and ions ($Q_i=0$); - - - - -, $\gamma_p=0$, and J_i as marked.

dary electrons at the cathode as the result of the arrival of photons, ions, and metastables. We can calculate the nd versus E/n curves for this model by neglecting atom- and ion-induced ionization in Eqs. (2)–(4) in Sec. III and solving the equations as outlined in the Appendix. A representative result for $\gamma_p=0.05$ and $Q_p^i=Q_f^i=0$ is shown in Fig. 11 by the single-link chain curve for 4 kTd $< E/n < 20$ kTd and by the solid curve for $E/n < 4$ kTd. This curve shows that one can obtain approximate agreement between the electron-impact model and experiment for E/n from the lowest value considered, 200 Td, to about 4 kTd for a single reasonable⁵⁰ value of γ_p . As the E/n is increased beyond 4 kTd, γ_p would have to be increased rapidly. At extremely large E/n one would need very large values of γ_p , e.g., 7 at 300 kTd. This value is about an order of magnitude higher than the largest measured⁵⁰ value for Ar⁺ at the calculated energy of $kT_+ \approx 1000$ eV. We calculate that about three fast atoms per ion reach the cathode for these conditions, so that the yield of secondary electrons per atom⁴³ would have to be at least several times that measured for ions⁵⁰ in order for ion and fast-atom bombardment to supply the necessary electrons. The necessary high electron yields seem unlikely, so that the traditional electron production terms do not appear adequate to explain experiment at the higher E/n .

A number of discussions⁵¹ and models⁵ of breakdown at very high E/n have included the effects of electrons backscattered from the anode. A complete treatment of this effect is beyond the scope of this paper. We can, however, obtain an upper limit to the contribution of backscattering to the ionization by electrons by using the model developed by Parker and co-workers,⁵ in which a fraction r of the electrons are reflected without loss of energy and so retrace the path of the primary electrons before turning around and returning to the anode. As discussed in Sec. II D of II, this approximation results in an increase in the ionization by electrons by a factor of $(1+r)/(1-r)$. In our present model this factor is multiplied by the first term on the right-hand side of Eq. (2). Using the estimate of Bhasavanich and Parker⁵ that $r=0.3$, we find that $\gamma_p \approx 4$ is required to fit their breakdown data at 300 kTd when ionization by fast atoms and ions is omitted. This value agrees well with the value of $\gamma_p=3$ obtained by Bhasavanich and Parker⁵ from analysis of their data. At 42.6 kTd, a γ_p value of about 0.5 would be required for this model to fit experimental breakdown data. We conclude that the addition of electron-backscattering to the electron-impact model does not lead to sufficient additional ionization to allow one to reduce the required γ_p to values consistent with beam experiments.⁵⁰ Furthermore, measurements⁴⁷ show that a value of $r \approx 0.1$ is more characteristic of carbon and that electron-energy losses at the anode are significant.

B. Ionization by electrons, ions, and atoms

We consider next the limiting case in which all of the electron production occurs by collisions of either electrons, fast atoms, or ions with Ar, i.e., the limit of zero

secondary electron emission from the cathode. This model is basically an extension of Townsend's⁵² original model of electrical breakdown to include the effects of ionization by fast neutral atoms. These calculations were carried out using the complete model expressed by Eqs. (2)–(13), analytical approximations to the electron-collision cross sections, the ion and fast-atom collision ionization and attenuation coefficients in Table I, and the coupled differential-equation code discussed in the Appendix. The values of nd versus E/n calculated using this model for $\gamma_p=0$ are shown by the short-dashed curves of Fig. 11. We see that for E/n between 15 and 50 kTd this model, which utilizes only gas-phase production of electrons and ions and has no adjustable constants, accounts reasonably well for the experimental-breakdown and discharge-maintenance data. At higher E/n the measured nd values fall below the dashed curve and other feedback processes must be included in the model. Using this model to calculate the electron-current multiplication, $\Gamma_e(nd)/\Gamma_e(0)$, we conclude that for $E/n > 20$ kTd and for nd corresponding to breakdown the ionization is produced primarily in collisions of fast atoms and ions with Ar rather than by the electrons. As an example, at $E/n = 42$ kTd when the discharge voltage is kept the same and α_f'/n and α_p'/n are set to zero the electron current multiplication is reduced from 13 to less than 2.

The production of ions near the anode by backscattered or secondary electrons^{5,51} can be the dominant mechanism for electron-induced ionization of the gas at very high E/n . Evidence for the presence of such electrons in our experiments is provided by the excess emission discussed in Sec. IV A. In the present analysis an upper limit to the contribution of this ionization to breakdown will be obtained by replacing the integral of the spatially distributed ion production by an equivalent production at the anode $\Gamma_p^a(nd)$. Thus

$$\Gamma_p^a(nd) = \int_0^{nd} Q_e^i(\xi) \Gamma_b(\xi) d\xi. \quad (16)$$

Equations (2)–(13) are then solved with the total ion flux generated by backscattered electrons $\Gamma_p^a(nd)$ given by Eq. (16) as an anode boundary condition. The effects of this ion source on breakdown are seen in the plots of the nd values required for breakdown versus E/n shown in the upper right-hand corner of Fig. 11. Here the nd values have been multiplied by a factor of 100 in order to prevent overlapping curves. The parameter for these plots is the equivalent ion current density at the anode normalized to the total current density $J_i \equiv \Gamma_p^a(nd)/\Gamma_t$. These calculations were made assuming that the ion-induced secondary electron yield at the cathode γ_p is zero. We see that for $E/n > 20$ kTd one can fit even the lowest set of nd values with only a 20% yield of ions per electron striking the anode.

Estimates of the efficiency of ion production near the anode can be made from the calculations of Sec. III D of II. From these calculations we estimate the efficiency of ionization per electron reflected from the anode to be of the order of unity and to vary slowly with E/n . Considering the range of measured backscattering yields⁴⁷ and

the shortage of energy-distribution data discussed in Sec. IV A, we can only roughly estimate the ion-flux yield J_i for graphite to be a few percent of the incident-electron flux.⁵³ Values of J_i are expected to be significantly higher for metals,⁴⁷ so that $J_i \approx 0.2$ may be reasonable for the experiments of Bhasavanich and Parker.⁵ These analyses show that ionization by backscattered electrons becomes more important at very high E/n , where ionization by high-energy electrons from the cathode end of the discharge is becoming less efficient.

C. Complete model

The solid curve in Fig. 11 shows an example of the results of calculations when all of the gas-ionization processes and ion-induced electron production at the cathode are included. To simplify the graph, results are shown for a single value of γ_p and of J_i . The solid curve shows that one only needs to adjust γ_p to ≈ 0.05 to fit the lower- E/n data, while adjusting J_i to ≈ 0.05 to fit the higher- E/n data. Of course, this fit does not rule out increases in γ_p with increasing E/n . Some idea of the sensitivity to the choices of J_i and γ_p is obtained by noting that doubling γ_p to 0.1 would reduce the nd values by about 20% for $E/n < 5$ kTd, but would have a negligible effect for $E/n > 50$ kTd. A γ_p value of 0.5 would be required to reduce nd by 10% at $E/n = 1000$ kTd. The value of $J_i = 0.05$ was chosen to fit our discharge-maintenance data (Sec. II) and the breakdown data of Guseva⁴⁹ for $5 < E/n < 1000$ kTd. A J_i value of about 0.2 would be required to fit the very-high- E/n data of Bhasavanich and Parker.⁵ An alternate way to fit these low- nd values is to keep $J_i \approx 0.05$ and increase γ_p to values of 3 to 5. Presumably, the best model would be intermediate between these two limits. We conclude that by including gas ionization by ions and fast atoms and by backscattered electrons in the model of breakdown in Ar, we can fit the published data with reasonable ion-induced secondary emission coefficients and backscattered-electron yields.

The success of the analysis of Ar-breakdown data presented in this section suggests that ionization by fast atoms and ions is responsible for the higher-voltage portions of the multiple-valued curve of breakdown voltage versus nd found^{12,49} for He and the highly structured curves found⁴⁹ for Ne and for Hg. When plotted as in Fig. 11, the experimental multiple valued curve for He translates into a curve with a maximum value of nd at $E/n = 3$ kTd. The Ne data shows an even more pronounced break near $E/n = 10$ kTd than does the Ar curve in Fig. 11. Although we have not extended the detailed analysis carried out for Ar to these gases, we second the suggestion of Druyvesteyn and Penning¹² that the high- E/n portions of these curves are dominated by fast-atom- and ion-induced ionization. The maximum in nd versus E/n for He would appear to result from a large separation of the E/n ranges for which electron-induced ionization dominates and that for which heavy-particle collisional ionization dominates the ionization. In the case of Ar, these E/n ranges are less widely separated and no maximum is observed.

VI. DISCUSSION

The experiments and models presented in this paper cover the transition from moderate E/n , where the electrons are in collisional equilibrium with the electric field and the gas and the ion energies are only a few times thermal, to very high E/n , where the electrons have few collisions with the gas and the ion and fast-atom energies are large enough to yield significant excitation and ionization. At E/n below 1 kTd the observed magnitude and spatial dependence of the 811-nm emission are consistent with the excitation and ionization expected of electrons in equilibrium with the electric field and collisions with the gas. At E/n between 1 and 10 kTd excitation and ionization by electrons is dominant toward the anode, although the electron behavior is best described by a nonequilibrium model. At E/n above 20 kTd, electron excitation is apparent only near the anode, where backscattered electrons are present. The excitation of 811-nm emission by fast atoms becomes important near the cathode at E/n of between 2 and 6 kTd. At the $E/n > 20$ kTd the spatial dependence of the observed excitation over most of the discharge gap is consistent with excitation by collisions between fast-Ar and Ar-gas atoms, where the fast Ar is produced in charge-transfer collisions of Ar^+ with the gas. Excitation of 811-nm radiation by fast ions appears to be small or negligible.

There are serious discrepancies among the various measures of the 811-nm excitation by electrons. Firstly, at low E/n the electron excitation coefficients we calculate from the cross sections determined in beam experiments^{23,25} are much larger than the directly measured excitation coefficients of Tachibana.¹⁶ Secondly, at our highest E/n the apparent excitation coefficients calculated using our model for the excess emission near the anode by backscattered electrons are much smaller than the experimental values. On the other hand, there is good agreement between the calculated apparent electron excitation coefficients and experiment at the intermediate E/n of 6.3 kTd. Although the variation of these discrepancies with gas density is roughly that expected if the quenching of the $2p_n$ states by Ar were much larger than previously determined,²⁰ the quenching-rate coefficient required, $> 5 \times 10^{-15} \text{ m}^3/\text{s}$, is much too large to have been missed. Support for the conclusion of Sec. III that quenching is small has been obtained from transient measurements of 811-nm emission in this laboratory.⁴ A possible explanation for the discrepancy near the anode at high E/n is that we have greatly underestimated the cascade contribution to electron excitation of the 811-nm lines. Absolute intensity measurements and measurements of emission from Ar lines sensitive primarily to electron excitation should help resolve these questions.

The analyses of breakdown and low-current discharge-maintenance voltage data presented in this paper demonstrate the importance of ionization of Ar by fast atoms and ions. It is important to note that no fitting parameters were used in the calculations of the ionization of Ar by the electrons, Ar^+ , and fast Ar. The data and analyses also show the probable importance of ionization of the Ar by backscattered electrons in the region near the anode as source of ions for discharge current growth and

steady-state discharge maintenance at the highest E/n .

The experiments and analyses presented in this paper lead to several suggestions for further experiments. One of these is the observation of the time dependence of spectrally and spatially resolved emission. Such observations have been carried out for the 811- and 750-nm lines of Ar by Scott and Phelps.⁴ Their partially analyzed results are consistent with the processes proposed in the present paper and provide additional evidence for the importance of collisions of fast Ar with the background Ar. Other suggested experiments are the measurement of the Doppler shift of radiation scattered by the Ar metastables produced by electrons or by heavy particle excitation, and the observation of emission versus position in steady-state experiments as the discharge current is increased to the region where space-charge distortion of the electric field becomes important. The cross section sets presented in this paper for Ar^+ and Ar collisions with Ar are available on request.⁵⁴

ACKNOWLEDGMENTS

The authors would like to acknowledge many helpful discussions with A. Gallagher. They would like to thank R. W. Weppner, J. Fenney, and S. Lissaur for help with the drift tube, the preparation of the computer, and development of electronics, respectively. This work was supported in part by the Lawrence Livermore National Laboratory.

APPENDIX: DETAILS OF THE MODEL

The purpose of this appendix is to present some details of the model of electron, Ar^+ , and fast-Ar behavior used in the comparison with experiment in Sec. IV. The calculations shown in Figs. 3-4, and 8-10 were carried out using momentum-transfer, excitation, and ionization cross sections for electrons from the source cited in Sec. II A and for Ar^+ and fast Ar from the sources cited in Sec. III B. The values of the ionization and excitation coefficients calculated from the cross sections of Fig. 6 using Eqs. (7) and (8) are given in Table I for the E/n of Figs. 8-10. The values of the spatial excitation coefficients required to give a good fit to experiment, the experimental values of nd , and the ratio of fast neutral to ion flux at the cathode are given in Table II.

In the original approach to the solution of Eqs. (2)-(13) we used tabulated cross sections for the electron collisions with Ar and simplified Eqs. (2) and (3) by the omission of the terms representing ionization of Ar by Ar^+ and fast Ar. Because of the simplicity of Eqs. (2) and (3), the solution of the resulting equations is that given in Sec. II A of II. These numerical results were then substituted into integral forms of the solutions of Eqs. (4) and (5).

In order to speed up the calculations and include all of the ionization terms in Eqs. (2) and (3), the tabular electron collision cross sections were replaced with analytical approximations.^{22,24} The coefficients listed in Table I were used for the Ar^+ and fast-Ar collision processes except that those of Table II were used for 811-nm excitation in Ar-Ar collisions. The equations were solved using a nonlinear, coupled, first-order differential-equation code

which integrates from one electrode to the other.⁵⁵ The number of final conditions to be met were minimized by starting at the anode. The initial conditions were $\Gamma_e(nd)/\Gamma_i = J_i$, $\Gamma_p = \Gamma_f = 0$, where J_i is discussed in Sec. VB. The electron energy at the anode $\epsilon(nd)$ was chosen iteratively such that the cathode boundary conditions of $\epsilon(0) = 1$ and $J_e(0)/J_i = \gamma_p/(1 + \gamma_p)$ were satisfied when $\int_0^{nz} dz E = V_d$, where the V_d values are shown in Fig. 1. At 42.6 kTd these calculations show that the inclusion of the Ar⁺- and fast-Ar-induced ionization terms in Eqs. (2) and (3) increases the calculated apparent excitation

coefficient near the cathode by about 20% over the values calculated when these terms are omitted. This increase is small compared to the calculated increase in the electron-current multiplication from cathode to anode of a factor of 7 when ionization by fast atoms and ions is added at fixed nd . The reduced importance of heavy-particle ionization in the calculated emission relative to its importance in calculated current multiplication is due to the fact that the emission data is normalized to the total discharge current, rather than to the cathode current as in the case of the current multiplication.

*Also at Quantum Physics Division, National Bureau of Standards, Boulder, CO 80303 and Physics Department, University of Colorado, Boulder, CO 80309.

†Present and permanent address: Institute of Physics, P.O. Box 57, Belgrade, Yugoslavia.

¹B. M. Jelenković and A. V. Phelps, *Phys. Rev. A* **36**, 5310 (1987).

²A. V. Phelps, B. M. Jelenković, and L. C. Pitchford, *Phys. Rev. A* **36**, 5327 (1987). The values cited after Eq. (18) in this reference of 70 and 170 eV m² should be multiplied by 10⁻²¹. The values cited in the text were correctly used in calculations in which the E/n values were in Td. In the expression for $f(v, \theta, z)$ between Eqs. (1) and (2) the N^2 should be v^2 .

³Short reports on some of this work have been published. See B. M. Jelenković and A. V. Phelps, *Bull. Am. Phys. Soc.* **32**, 1143 (1987); in *Proceedings of Conference on the Physics of Ionized Gases, Sebenik, Yugoslavia, 1986*, edited by M. V. Kurepa (University of Belgrade, Belgrade, 1986); A. V. Phelps, *Invited Papers from the International Conference on Ionization Phenomena in Gases*, edited by W. T. Williams (Hilger, Bristol, 1987), p. 2. The estimates of 811-nm excitation by electrons in Fig. 6 of the latter reference are superseded by those of the present paper.

⁴D. A. Scott and A. V. Phelps, *Bull. Am. Phys. Soc.* **32**, 1158 (1987).

⁵J. D. Pace and A. B. Parker, *J. Phys. D* **6**, 1525 (1973); D. Bhasavanich and A. B. Parker, *Proc. R. Soc. London, Ser. A* **358**, 385 (1977).

⁶W. D. Davis and T. A. Vanderslice, *Phys. Rev.* **131**, 219 (1963); A. V. Bondarenko, *Zh. Tekh. Fiz.* **43**, 821 (1973) [*Sov. Phys.—Tech. Phys.* **18**, 515 (1973)].

⁷K. N. Ul'yanov, *Teplofiz. Vys. Temp.* **16**, 1121 (1978) [*High Temp. (USSR)* **16**, 955 (1978)]; K. N. Ul'yanov and A. B. Tskhai, *Teplofiz. Vys. Temp.* **19**, 41 (1981) [*High Temp. (USSR)* **19**, 32 (1981)].

⁸D. G. Armour, H. Valisadeh, F. A. H. Soliman, and G. Carter, *Vacuum* **34**, 295 (1984).

⁹R. T. C. Tsui, *Phys. Rev.* **168**, 107 (1968); I. Abril, A. Gras-Marti, and J. A. Valles-Abarca, *Phys. Rev. A* **28**, 3677 (1983); *J. Phys. D* **17**, 1841 (1984); J. Rickards, *Vacuum* **34**, 559 (1984).

¹⁰J. E. Lawler, *Phys. Rev. A* **32**, 2977 (1985).

¹¹W. H. Long, Jr., Air Force Aeronautical Laboratories Report No. AFAPL-TR-79-2038, 1979 (unpublished); H. Chatham and A. Gallagher, *J. Appl. Phys.* **58**, 159 (1985).

¹²M. J. Druyvesteyn and F. M. Penning, *Rev. Mod. Phys.* **12**, 87 (1940); M. Hayashi, *J. Phys. D* **15**, 1411 (1982); J. Fletcher, *ibid.* **18**, 221 (1985).

¹³H. Mase, T. Tanabe, K. Taneko, and G. Miyamoto, *J. Phys. D* **12**, L123 (1979); P. P. Ong and M. J. Hogan, *J. Phys. B* **18**, 1897 (1985). The theory cited by M. J. Hogan and P. P. Ong, *J. Phys. B* **19**, 2123 (1986) is not applicable to cases where symmetric charge transfer is dominant, such as Ar⁺ in Ar. See Ref. 10 and H. Wallman, E. A. Mason, and L. A. Viehland, *Chem. Phys.* **66**, 339 (1982).

¹⁴W. L. Wiese, M. W. Smith, and B. M. Glennon, *Atomic Transition Probabilities* (U.S. Department of Commerce, Washington, D.C., 1966), Vol. 1, p. 192.

¹⁵V. Kempter, F. Vieth, and L. Zehnle, *J. Phys. B* **8**, 2835 (1975); V. Kempter, G. Rieke, F. Vieth, and L. Zehnle, *ibid.* **9**, 3081 (1975).

¹⁶K. Tachibana, *Phys. Rev. A* **34**, 1007 (1986).

¹⁷F. M. Penning and C. C. J. Addink, *Physica (Utrecht)* **1**, 1007 (1934).

¹⁸F. J. De Hoog and J. Kasdorp, *Physica (Utrecht)* **34**, 63 (1967); A. K. Bhattacharya, *Phys. Rev.* **13**, 1219 (1976); *J. Appl. Phys.* **50**, 6207 (1979).

¹⁹A. A. Kruithof, *Physica (Utrecht)* **7**, 519 (1940); J. Dutton, *J. Chem. Phys. Ref. Data* **4**, 577 (1975); R. R. Abdulla, J. Dutton, and A. W. Williams (unpublished).

²⁰R. S. F. Chang and D. W. Setser, *J. Chem. Phys.* **69**, 3885 (1978). See also T. D. Nguyen and N. Sadeghi, *Phys. Rev. A* **18**, 1388 (1978); A. Catherinot, P. Placidet, and B. Dubreuil, *J. Phys. B* **11**, 3775 (1978).

²¹M. Hayashi, Institute of Plasma Physics, Nagoya University, Report No. IPPJ-AM-19, 1981 (unpublished).

²²D. Rapp and P. Englander-Golden, *J. Chem. Phys.* **43**, 1464 (1965); B. L. Schramm, F. J. De Heer, M. J. van der Wiel, and J. Kistnermacher, *Physica (Utrecht)* **31**, 94 (1965). The approximation to the ionization cross section used is $Q_i^e = 1.1 \times 10^{-17} (\epsilon - 15.8) / (100 + \epsilon)^2$ m², where ϵ is in eV.

²³J. K. Ballou, C. C. Lin, and F. E. Fajen, *Phys. Rev. A* **8**, 1797 (1973). Note that the use of the 811.5-nm optical cross section from this reference yields excitation coefficients about four times those shown by the solid curve of Fig. 3. The reason for this discrepancy is unknown. If we were to reduce these cross sections so as to yield excitation coefficients consistent with those of Ref. 16, the discrepancy between the electron-excitation model for the excess emission near the anode and experiment would be even larger than indicated in Sec. IV A.

²⁴L. R. Peterson and J. L. Allen, Jr., *J. Chem. Phys.* **56**, 6068 (1972). The approximation to the energy loss function used is $L(\epsilon) = 4 \times 10^{-16} (\epsilon - 12) / (100 + \epsilon)^2$ m².

²⁵A. Chutjian and D. C. Cartwright, *Phys. Rev. A* **23**, 2178 (1981). The cross sections obtained by these authors for the

- $2p_7$ and $2p_9$ levels agree with those of Ref. 23 at 30 eV, but are very much lower at other energies.
- ²⁶R. Hergerberg, M. T. Elford, and H. R. Skullerud, *J. Phys. B* **15**, 797 (1982). For summaries of published data see E. W. McDaniel, *Collision Phenomena in Ionized Gases* (Wiley, New York, 1964), Fig. 6-2-6; E. Salzbom, *IEEE Trans. Nucl. Sci. NS-23*, 947 (1976).
- ²⁷Th. J. M. Sluyters, E. De Hass, and J. Kistmacher, *Physica (Utrecht)* **25**, 1376 (1959).
- ²⁸R. C. Isler and L. E. Murray, in *Electronic and Atomic Collisions*, edited by J. S. Risley and R. Geballe (University of Washington, Seattle, 1975), Vol. 2, p. 609.
- ²⁹Th. J. M. Sluyters and J. Kistmacher, *Physica (Utrecht)* **25**, 1389 (1959); S. H. Neff, *Astrophys. J.* **140**, 348 (1964).
- ³⁰E. W. Thomas, *Excitation in Heavy Particle Collisions* (Wiley-Interscience, New York, 1972), p. 178.
- ³¹E. G. Jones, Air Force Aeropropulsion Laboratory Report No. AFAPL-TR-78-99, 1978 (unpublished); *Phys. Rev. A* **21**, 1902 (1980); (private communication).
- ³²P. O. Haugsjaa, R. C. Amme, and N. G. Utterback, *Phys. Rev. Lett.* **22**, 322 (1969). The theory of such excitation processes is discussed in, for example, V. Sidis, M. Barat, and D. Dhuicq, *J. Phys. B* **3**, 474 (1975).
- ³³H. C. Hayden and R. C. Amme, *Phys. Rev.* **141**, 30 (1966); R. H. Hammond, J. M. S. Henis, E. F. Greene, and J. Ross, *J. Chem. Phys.* **55**, 3506 (1971).
- ³⁴P. O. Haugsjaa and R. C. Amme, *J. Chem. Phys.* **52**, 4874 (1970).
- ³⁵R. S. Robinson, *J. Vacuum Sci. Technol.* **16**, 185 (1979).
- ³⁶V. Neuman, *Ann. Phys. (Leipzig)* **34**, 603 (1939).
- ³⁷P. O. Haugsjaa and R. C. Amme, *Phys. Rev. Lett.* **23**, 633 (1969); H. L. Rothwell, Jr., R. C. Amme, and B. Van Zyl, *ibid.* **36**, 785 (1976); *Phys. Rev.* **19**, 970 (1979).
- ³⁸T. I. McLaren and R. M. Hobson, *Phys. Fluids* **11**, 2162 (1968). Using detailed balancing arguments and measured Ar metastable two-body destruction rate coefficients, we conclude that these cross sections are much too large. For Ar metastable-destruction data see, for example, J. H. Klots and D. W. Setser, *J. Chem. Phys.* **68**, 4848 (1978). Similar conclusions have been reached by W. Botticher, in *Invited Papers from the International Conference on Ionization Phenomena in Gases*, edited by W. T. Williams (Hilger, Bristol, 1987), p. 10.
- ³⁹J. C. Brenot, D. Dhuicq, J. P. Gauyacq, J. Pommier, V. Sidis, M. Barat, and E. Pollack, *Phys. Rev. A* **11**, 1245 (1973).
- ⁴⁰J. P. Gauyacq, *J. Phys. B* **11**, 85 (1978).
- ⁴¹H. W. Ellis, R. Y. Pai, E. W. McDaniel, E. A. Mason, and L. A. Viehland, *At. Data Nucl. Data Tables* **17**, 177 (1976).
- ⁴²J. P. Molnar, *Phys. Rev.* **83**, 940 (1951).
- ⁴³K. Kadota and Y. Kaneko, *Jpn. J. Appl. Phys.* **13**, 1554 (1974).
- ⁴⁴R. Kollath, in *Electron Emission. Gas Discharges I*, Vol. XXI of *Handbuch der Physik* (Springer, Berlin, 1956), p. 232.
- ⁴⁵M. E. Woods, B. J. Hopkins, and G. M. McCracken, *Surf. Sci.* **162**, 928 (1985).
- ⁴⁶The numerically calculated yield of 811-nm photons per backscattered electron traveling normal to the anode and including cascade excitation can be approximated by $20(\epsilon_b)^{1/2}/(E/n)$, where ϵ_b is the energy of the backscattered electron in eV and E/n is in Td. The corresponding yield of ions is approximately $35\epsilon_b/(E/n)$. The reduction in the yields with increasing E/n is due to the compression of the range of nz in which electron excitation or ionization can occur. These yields of excited atoms and ions per electron are obtained by integration of excitation and ionization coefficient curves versus distance similar to those in Fig. 5 of II. One reason for the low yields of excited states and ions is that most of the electron energy is returned to the anode with the electron, i.e., very little energy is dissipated in the gas per transit. The increased path lengths of electrons emitted at an angle to the normal will increase the yields and decrease the distance normal to the cathode before turn around. The increased yield is probably less than a factor of 2.
- ⁴⁷E. J. Sternglass, *Phys. Rev.* **95**, 345 (1954); E. H. Darlington and V. E. Cosslett, *J. Phys. D* **5**, 1969 (1972); R. L. Verma, *J. Phys. D* **10**, 1167 (1977). Note that while these results agree reasonably well for incident electron energies near 1 keV, they are spread over almost an order of magnitude for 500-eV electrons.
- ⁴⁸Calculated using $J_i=0.05$ and the excitation coefficient of Table II.
- ⁴⁹L. G. Guseva, in *Investigations into Electrical Discharges in Gases*, edited by B. N. Klyarfel'd (Pergamon, New York, 1964), pp. 1-11. Note that the multiple-valued curve shown in this reference for Hg has been the subject of disagreement. See M. J. Schönhuber, *IEEE Trans. Power Appar. Syst.* **PAS-88**, 100 (1969); P. C. Johnson and A. B. Parker, *Proc. R. Soc. London, Ser. A* **325**, 529 (1971); J. H. Stamer, *Beitr. Plasmaphys.* **13**, 79 (1973). In any case the data appear to have two distinct regions of ionization as for Ar, Ne, and He.
- ⁵⁰J. M. Parker, Jr., *Phys. Rev.* **93**, 1148 (1954); P. Mahadevan, J. K. Layton, and D. B. Medved, *ibid.* **129**, 79 (1963); G. D. Magnuson and C. E. Carlston, *ibid.* **129**, 2409 (1963).
- ⁵¹B. N. Klyarfel'd and L. G. Guseva, *Zh. Tekh. Fiz.* **35**, 306 (1965) [*Sov. Phys.—Tech. Phys.* **10**, 244 (1965)]; B. N. Klyarfel'd, L. G. Guseva, and V. V. Vlasov, *ibid.* **38**, 1288 (1968) [**13**, 1056 (1969)]. Low current, discharge maintenance experiments by this group require γ_p values of ≈ 0.1 . See B. N. Klyarfel'd, L. G. Guseva, and A. S. Pokrovskaya-Soboleva, *ibid.* **36**, 704 (1966) [**11**, 520 (1966)].
- ⁵²For a review of Townsend's model, see L. B. Loeb, *Fundamental Processes of Electrical Discharge in Gases* (Wiley, London, 1939), pp. 372-386. Our model differs from Townsend's in that in our case the electron-induced ionization coefficient varies with position and that most of the heavy-particle ionization is produced by collisions of Ar with Ar rather than Ar^+ with Ar.
- ⁵³An alternate procedure for estimating J_i at 42.6 kTd is to use (from Sec. IV A) the calculated ratio of ion to excited-state production, including cascading, of about 30 to 1 for the 350 eV secondaries and the experimental value of the integrated excess emission from of about 0.008 photon per electron striking the anode. This procedure yields J_i of about 0.2 ion per electron incident on the anode, which is too high.
- ⁵⁴A. V. Phelps, Joint Institute for Laboratory Astrophysics Information Center Report No. 33, 1988 (unpublished). This report also includes similar cross section and bibliographic compilations for H_2 and N_2 .
- ⁵⁵D. K. Kahnaher, E. Agron, D. Barnett, and C. Gunaratna, *IEEE Micro* (to be published).